J. Fluid Mech. (1968), *vol.* 31, *part* 1, *pp.* 163–174
Printed in Great Britain

Impingement of gas jets on liquid surfaces

By RICHARD S. ROSLER AND GEORGE H. STEWART

Department of Chemistry and Chemical Engineering,
Gonzaga University, Spokane, Washington

(Received 23 June 1967)

An investigation of the interaction of a jet of air impinging normally on a liquid surface has been carried out. The regimes of stable, oscillating, and dispersing indentions were established as a function of velocity and surface tension.

For the stable region, energy and force balances were formulated. The force balance, when integrated, described the indention profile well and will have further use in predicting the point of onset of instability.

A linear relationship between the square of the instability velocity and the surface tension and between the square of the critical dispersion velocity and the surface tension has been determined experimentally.

1. Introduction

A jet of gas impinging on the surface of a liquid with sufficient momentum to disperse liquid droplets from the surface serves as a system suitable for study of liquid dispersion in more complex systems. This model system with its simplicity and its symmetry properties allows the study of a wide range of gas liquid interactions. Other investigators have used a similar system for the study of oxygen transport into the liquid system in analogy with the manufacture of steel (Collins & Lubanska 1954; Mathieu 1960, 1962) and to study the properties of a spreading turbulent jet (Turkdogan 1966). The system has also been proposed by Pfund & Greenfield (1936) as a method of measuring liquid surface tensions.

This investigation derives from the authors interest in that regime of gas–liquid two-phase flow known as dispersed flow. The physical parameters of the liquid which control the onset of dispersion in two-phase flow have received little attention and the impinging jet provides a model in which the various parameters are independently variable and the symmetry of the system holds some promise for an analytical approach. In this study, the interaction between the jet and the liquid is characterized up to jet velocities causing dispersion. The influence of the surface tension of the liquid is determined and compared with the model analysis.

A column of gas impinging on a liquid surface causes an indention of the liquid surface. At low gas velocities (refer to figure 1) a steady-state configuration of the liquid surface is attained and the indention has cylindrical symmetry. As the momentum of the jet increases the indention becomes deeper and approaches the length to width ratio at which the system becomes unstable. The velocity at

which the indention becomes unstable, u_{inst}, is marked by oscillations of the indention which become more vigorous with a further increase in gas velocity. With the further increase of the momentum of the gas stream a velocity is reached where the vigorous oscillation of the indention disperses bubbles of gas into the liquid and at slightly higher velocities there is a dispersion of liquid droplets into the air. The latter, liquid dispersion, is rather well characterized by the velocity of the gas stream at the onset of dispersion, u_{crit}, as the onset of instability is characterized by u_{inst}.

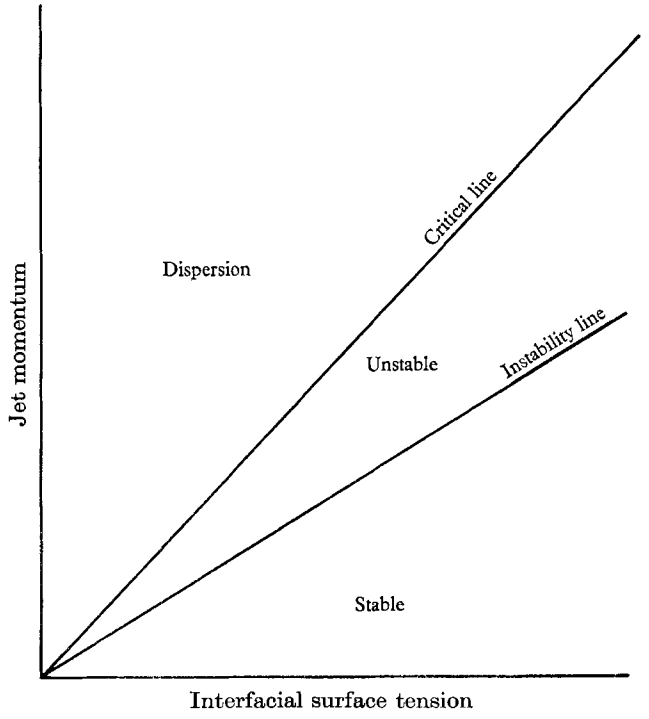

FIGURE 1. Regimes of the indention as characterized by jet momentum versus interfacial surface tension.

Previous analyses of an air jet impinging on a liquid surface have concentrated on the development of an expression for the centreline depth of the depression. Banks & Chandrasekhara (1962) found good agreement with experiment for their force balance between the dynamic pressure at the jet centreline, the indention buoyancy (which involves the centreline indention depth), and a surface tension radius of curvature term. Turkdogan (1966) recently carried out a similar study but did not include the surface tension term. Both studies were concerned with the variation of indention centreline depth as a function of jet radius and velocity and the distance of the jet exit from the liquid surface. Neither considered the effect of surface tension in detail. Our interest is specifically directed toward discovery of the role of surface tension.

2. Theory: steady state

Energy balance

It is the purpose of this section to formulate an overall indention energy balance. The momentum flux of each cylindrical shell of gas impinging on the liquid acts through an average distance, $\bar{h}$, which is approximately the depth of the indention of the liquid surface. Some fraction, K, of this work summed over the complete cross-section of the jet appears as the potential energy of the indention. For laminar flow at the capillary exit

$$w_1 = \tfrac{4}{3} K \pi R_c^2 \rho_g u_{\mathrm{av}}^2 \bar{h} \tag{1a}$$

and for highly turbulent flow (flat velocity profile)

$$w_1' = K' \pi R_c^2 \rho_g u_{\mathrm{av}}^2 \bar{h}, \tag{1b}$$

where R_c is capillary radius, ρ_g is air density, and u_{av} is the average velocity at the capillary exit.

The energy transferred from the gas stream appears in the liquid in three forms: a displacement of the liquid (gravitational energy), motion in the liquid (kinetic energy) and an increase of the surface area of the liquid (surface energy). For this analysis the energy due to motion in the liquid is neglected. Since the indention of the liquid has a cylindrical symmetry, the buoyancy term is the sum of the displacement energy of circular plates of liquid of differential thickness, dh, through a distance h,

$$\epsilon_2 = \int_0^{h_0} h(\rho_1 - \rho_g)\, g \pi r^2\, dh \equiv h_{cg}(\rho_1 - \rho_g)\, g V, \tag{2}$$

where ρ_1 is the liquid density, g is gravitational acceleration, r is the indention radius at h, and V is the indention volume. The net surface created is the surface area of the indention less the surface of the undisturbed liquid,

$$\Delta A = A_{\mathrm{ind}} - A_{\mathrm{orig}}.$$

The surface energy term is the product of the net surface and the surface tension, σ,

$$\epsilon_3 = \sigma \Delta A. \tag{3}$$

At this point an energy balance may be written as follows:

$$w_1 = \epsilon_2 + \epsilon_3. \tag{4}$$

This balance applies in the region where indention oscillations have not yet begun. The substitution of equations (1*a*), (2) and (3) into (4) gives upon rearrangement (for laminar flow in capillary)

$$u_{\mathrm{av}}^2 = \frac{1}{4/3 K \pi R_c^2 \rho_g} \left[\frac{\Delta A}{\bar{h}} \sigma + (\rho_1 - \rho_g)\, g \frac{h_{cg}}{\bar{h}} V \right]. \tag{5}$$

Force balance

An expression will now be developed which, when integrated with the pressure and interfacial shear stress distribution caused by the impinging jet, will describe

the total profile of the indention including the centreline depth. A sketch of the indention system is shown in figure 2. A force balance taken in the vertical direction on the element shown gives

$$2\pi r\,ds\,p\cos\alpha + 2\pi r\sigma\sin\alpha\big|_r = 2\pi r\,ds\,\tau\sin\alpha + 2\pi r\,dr(\rho_1-\rho_g)\,gh + 2\pi r\sigma\sin\alpha\big|_{r+dr}, \tag{6}$$

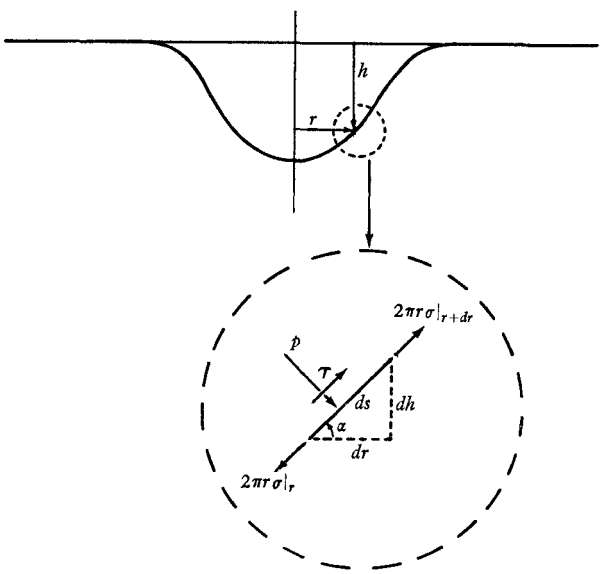

FIGURE 2. Indention system sketch for force balance derivation.

where p is the pressure difference across the interface and τ is the interfacial shear stress caused by the impinging jet flow. Substituting $dr/\cos\alpha$ for ds and taking the limit after dividing through by $2\pi r\,dr$ results in

$$p - \tau\tan\alpha = (\rho_1-\rho_g)\,gh + \frac{\sigma}{r}\frac{d}{dr}(r\sin\alpha). \tag{7}$$

Replacing the trigonometric functions by

$$\tan\alpha = -\frac{dh}{dr}, \quad \sin\alpha = \frac{-dh/dr}{[1+(dh/dr)^2]^{\frac{1}{2}}}$$

and rearranging after expanding the differentials gives

$$\frac{d^2h}{dr^2} + \frac{1}{r}\frac{dh}{dr}\left[1+\left(\frac{dh}{dr}\right)^2\right] = \frac{1}{\sigma}\left[(\rho_1-\rho_g)\,gh - p - \tau\frac{dh}{dr}\right]\left[1+\left(\frac{dh}{dr}\right)^2\right]^{\frac{3}{2}}. \tag{8}$$

Providing that the distributions of p and τ are known, equation (8) may be integrated numerically. The solution requires an iteration for the indention centreline depth since the boundary conditions are separated (i.e. at $r = 0$ $dh/dr = 0$ and at $r \to \infty$ both dh/dr and $h \to 0$).

An example of the type of pressure distribution used is (for laminar flow at capillary exit close to liquid surface):

$$p = 2\rho_g u_{\text{av}}^2 F \sin\left(1 - \frac{r}{\beta R_c}\right)\frac{\pi}{2}, \tag{9}$$

where $F = 1, \quad F = 0 \text{ to } 0{\cdot}03, \quad F = 0,$

$$0 \leqslant r/R_c < \beta, \quad \beta \leqslant r/R_c < 3\beta, \quad 3\beta \leqslant r/R_c.$$

This pressure distribution was chosen because it provides an adjustable negative pressure and is similar to that measured by Gibson (1934, p. 372) on a flat surface. A formulation of this type allows for the expected negative (relative to atmospheric) pressure near the high curvature upper part of the indention. For conservation of momentum, a force balance between the jet momentum and the surface pressure caused by it is written as

$$\tfrac{4}{3}\pi R_c^2 \rho_g u_{\text{av}}^2 = \int_0^\infty p\, 2\pi r\, dr = \int_0^{\beta R_c} p\, 2\pi r\, dr + \int_{\beta R_c}^{3\beta R_c} p\, 2\pi r\, dr. \tag{10}$$

Substituting equation (9) into (10) and integrating gives the necessary relationship between β and F:

$$\beta = [3(0{\cdot}231 - 2{\cdot}545F)]^{-\frac{1}{2}}. \tag{11}$$

The interfacial shear stress, τ, is approximated by

$$\tau = [\tfrac{1}{2}\rho_g u_{\text{av}}^2][0{\cdot}664/\sqrt{(Re_s)}][1 - e^{-(s/R_c)^2}], \tag{12}$$

where s is the distance along the interface from the centre of the indention and Re_s is the Reynolds number based on s.

3. Experiment

A diagram of the apparatus is shown in figure 3. Laboratory air was pumped by a diaphragm pump through a saturator filled with test fluid. Loss of liquid from the saturator during a test period was insufficient to alter the composition of the saturating liquids. The air was passed through a buffer volume of three four-litre containers which caught any entrained liquid from the saturator and also reduced fluctuations in pressure at the jet. The exiting gas was tested for saturation and found to average about 97 % saturation. The saturated gas passed from the buffer volume through an orifice meter previously calibrated with a wet test meter. Flow rates were adjusted by means of a by-pass valve. The gas was directed through a capillary tube (0·157 cm I.D. by 15·2 cm long) positioned 6·4 capillary diameters above the fluid. The test liquid was contained in a glass reservoir, 10 by 30 cm, which provided a width to capillary diameter ratio of 191. Reflexion of gas from reservoir walls did not modify the integrity of the jet and reflected waves were minimal.

The liquids used were ethanol–water mixtures as reported in table 1. This alcohol–water system was used as it allowed variation in surface tension with minimal variation in viscosity and density.

Stable indentions of the liquid surface were photographed using a Praktika 35 mm camera with Kodak Tri-X film (ASA 400) and two 150 watt spotlights. The projection of the image to an enlargement of 30 × enabled the indention

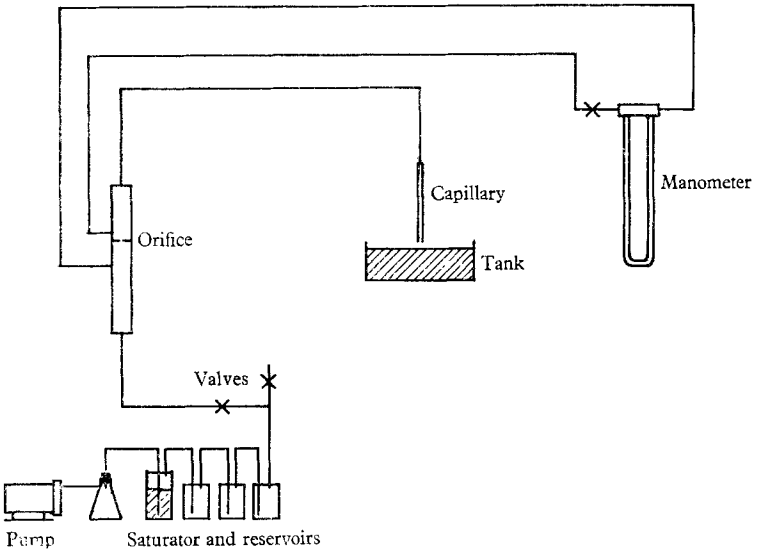

FIGURE 3. Diagram of apparatus.

Wt. % ethanol	Surface tension, 25 °C (dynes/cm)
0	72·0
2·72	60·8
5·21	54·9
11·10	46·0
20·50	37·5
40·00	29·6
87·92	23·6

TABLE 1.

profiles to be accurately measured. Using the indention profiles together with a digital computer (IBM 1130) program allowed calculation of $\Delta A, \bar{h}$, h_{cg} and V so that K could be calculated from equation (5). The evaluation of $\bar{h}$ is considered in the appendix.

The instability velocity and critical dispersion velocities were observed visually. These could be determined with a precision of $\pm 3\,\%$.

4. Results and discussion

Stable profile

Energy balance

At each of the seven surface tensions indicated in table 1, pictures were taken of the indention created by six different capillary velocities below u_{inst}. Repeat runs duplicating these conditions with new liquid mixtures of the same composition were made to establish reproducibility. One would expect the values of K (as K was defined in and prior to equation (1a)) to be in the region of unity depending to a large extent upon the angle through which the impinging jet stream is turned. Ideally, a turning angle of 90° would give $K = 1$ and one of 180° would yield $K = 2$. As seen in figure 4 where the highest and lowest surface tension cases are used in a plot of K *vs.* $(u_{\text{av}}/u_{\text{crit}})^2$, the experimental values of K range from 0·2 to 1·2. Intermediate values of surface tension give results between the two extremes shown.

The use of the energy balance expression, equation (5), to attempt a prediction of the relationship of u_{inst} to σ will be discussed below in the section devoted to unstable conditions.

Force balance

The comparison of the experimental and calculated indention profiles is shown in figures 5 and 6. In calculating the profiles, equation (8) was numerically integrated on an IBM 1130 computer with p and τ given by (9) and (12) and with $F = 0{\cdot}03$. Note that the prediction is not deep enough for the deep indention but too deep for the shallow indention. This indicates, as one would expect, that the relative magnitude of the negative pressure (as given by F) is larger for deep indentions than for shallow ones where the radius of curvature is much larger than that of the deep indention. The maximum value of τ that occurs is 0·5 % of the centreline p and is thus one-sixth of the maximum negative p. It should be pointed out that the indention is rather sensitive to F as a value of $F = 0$ for the deep indention reduces its depth by one-third.

The reasonable agreement of the theoretical profile with the experimental one indicates that the model adequately describes the steady-state indention phenomena. However, further work is necessary to express F as a function of velocity and indention shape and its possible dependence on surface tension and liquid viscosity. It will then be possible to extend the analysis to the point of predicting the instability line shown in figure 1 and discussed below.

Unstable indention

Instability and critical velocities

The experimental values of u^2_{inst} and u^2_{crit} are plotted as a function of surface tension in figure 7. The data for both the instability and the critical line were each taken on fresh fluid mixtures.

Since one would expect equation (5) to be applicable up to the point of instability an attempt was made to rationalize it to the experimental results. To determine the functionality of the variables $\Delta A/\bar{h}$, $Vh_{cg}/\bar{h}\sigma$, and K with σ at

the point of instability, each variable was plotted versus the square of the jet velocity for constant surface tension and then extrapolated to u^2_{inst}. The resulting $(\Delta A/\bar{h})_{\text{inst}}$, $(Vh_{cg}/\bar{h}\sigma)_{\text{inst}}$, and $(K)_{\text{inst}}$ were then plotted versus σ in figure 8. The points at the end of each vertical bar represent the values from two independent sets of measurements. A straight line is placed through the data and the

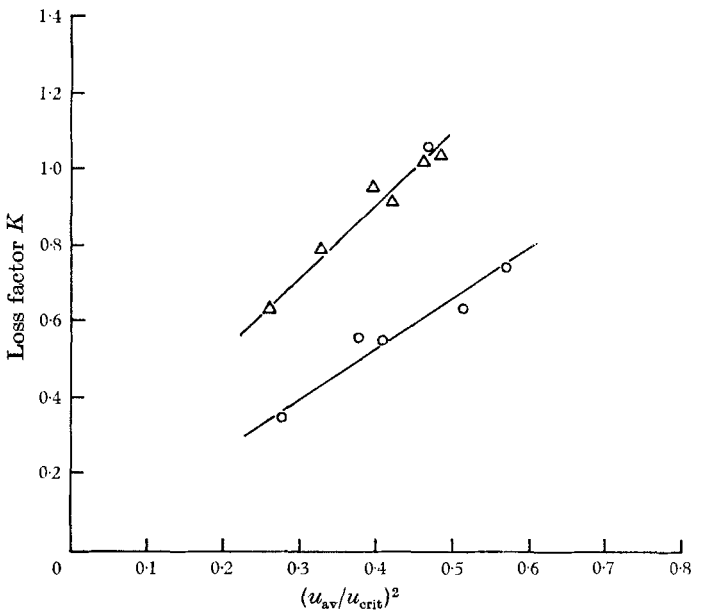

FIGURE 4. Loss factor, K, versus square of the ratio jet velocity to critical velocity for high and low surface tension cases. △, σ = 71·7 dynes/cm; ○, σ = 23·4 dynes/cm.

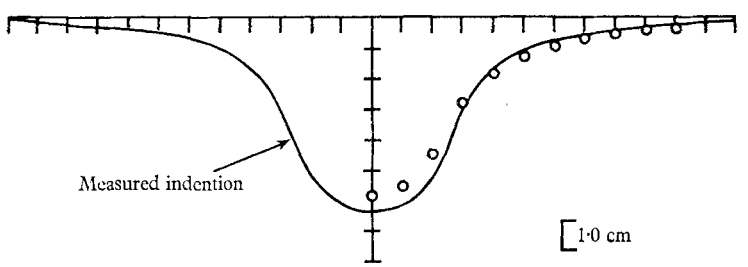

FIGURE 5. Calculated (σ = 71·5 dynes/cm) compared to measured indention profile: deep indention, enlarged by factor of 27·4.

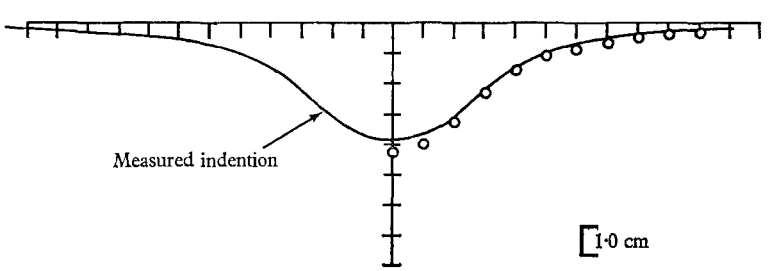

FIGURE 6. Calculated (σ = 71·7 dynes/cm) compared to measured indention profile: *shallow indention, enlarged by factor of* 27·9.

resulting expressions substituted into equation (5) which, after some manipulation, gives

$$u_{\text{inst}}^2 = 0{\cdot}188 \times 10^5 \frac{1 + 0{\cdot}0822\sigma}{1 + 0{\cdot}015\sigma}\,\sigma. \tag{13}$$

This, when plotted in figure 9, together with the instability data, is seen to be 15 to 20 % below experiment. A slight adjustment of the constants in equation (13) would give much better agreement with the data.

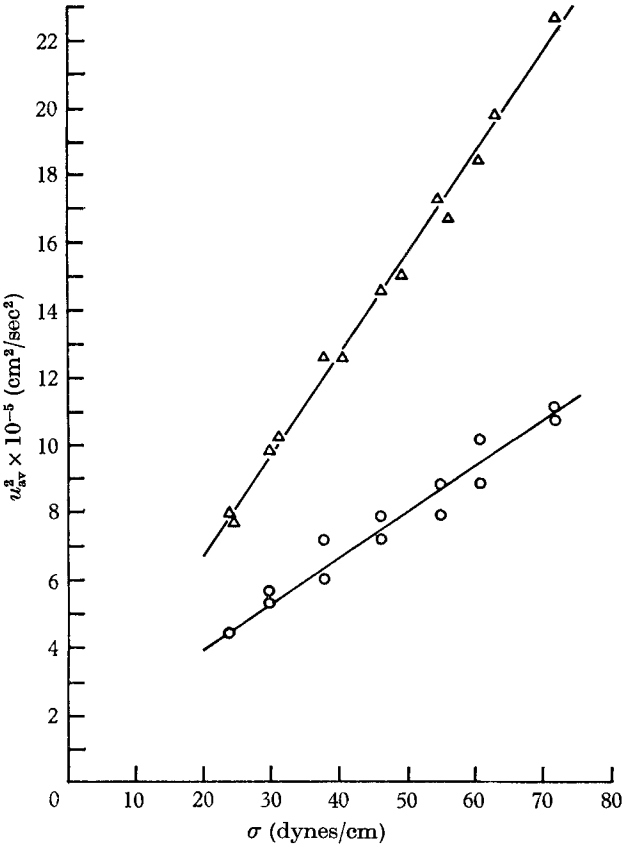

FIGURE 7. Square of critical and instability velocities versus interfacial surface tension. △, critical velocity; ○, instability velocity.

If an analogous approach is tried for the critical line the data are about 100 % above the resulting line. This stems from the fact that this approach of attempted extrapolation to the critical velocity, while highly inaccurate of itself, completely ignores the dynamical character of the indention in the instability region and the advent of new modes of utilization of momentum transfer from the impinging jet. These modes are discussed in the following section.

Instability and dispersion models

While the indention continues to grow with an increase of jet velocity above u_{inst}, a considerable energy absorption occurs in maintaining the motions of the indention. These motions may be categorized as: a stretching mode along the

axis of the jet, a bending mode, and rotation about the jet axis (see figure 10). The stretching mode must work against surface forces and is damped by viscous forces in the liquid. The bending mode changes surface shapes and expanse in the indention and also must work to buoy up the external surface of liquid. This work against the external surface leads to extensions of the external surface which, if of sufficient length, cause release of liquid droplets into the air. This is the major

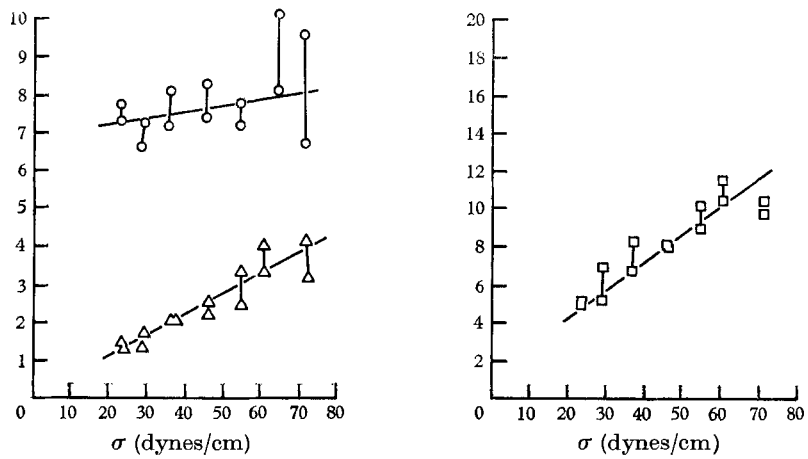

FIGURE 8. Parameters in equation (5) at point of instability versus interfacial surface tension. ○, $Vh_{cg}/\bar{h}\sigma$ (cm⁴/dyne) × 10^{-5}; △, $\Delta A/\bar{h}$ (cm) × 10^{-1}; □, loss factor, K × 10.

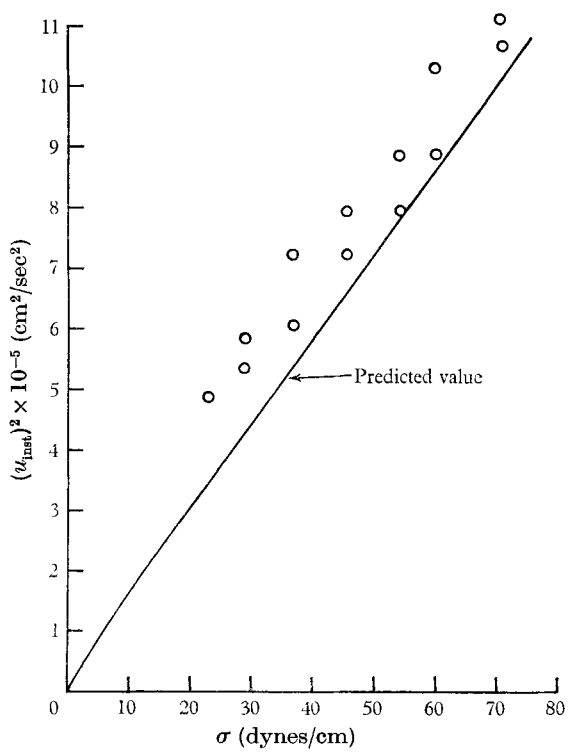

FIGURE 9. Extrapolated instability prediction of equation (13) compared with experimental data. ○, experimental data.

mechanism of dispersion. This bending mode of motion is also subject to viscous damping forces. The rotation of the indention (when bent from the axis) is subject to viscous forces.

From these observations, equation (5) must be modified by the addition of (if not by replacement by) a term of the form $B\sigma + C\mu$, where μ is the liquid viscosity. The equation for u_{crit} would then take the form:

$$u_{\text{crit}}^2 = u_{\text{inst}}^2 + B\sigma + C\mu. \tag{14}$$

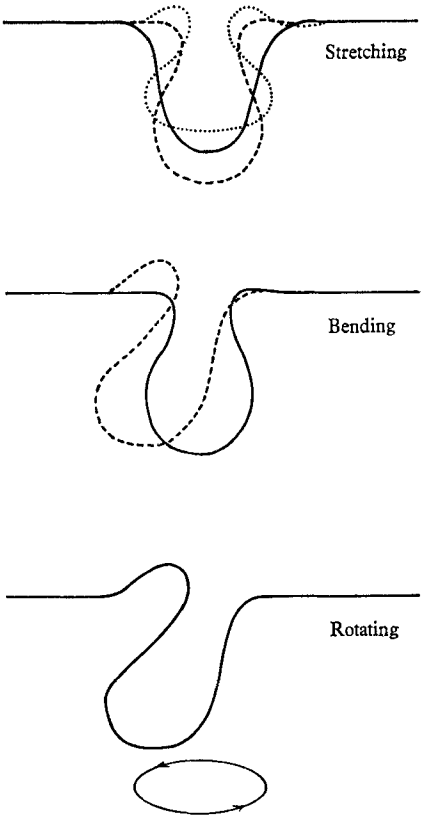

FIGURE 10. Modes of indention instability.

5. Summary

The regimes of stable, unstable, oscillating and dispersing indentions have been established as a function of velocity and surface tension.

For the region of the stable indention an overall energy balance, when evaluated using experimental data, is seen to be valid but to be of limited use due to the need to know the indention profile in order to evaluate most of the terms in the equation. A force balance gives a second-order differential equation, which, when integrated, predicts a steady-state indention profile. Further study is needed to determine the magnitude of the negative (relative to atmospheric) pressure near the indention periphery as a function of velocity and indention shape.

The instability and dispersed flow regimes were described qualitatively. It is expected that, after suitable criteria for the onset of instability have been established, the steady-state indention profile equation can be used to predict the velocity at which onset of instability will occur.

The onset of these regimes is given in figure 7 for liquids with a viscosity of about one centipoise and a capillary of 0·157 cm I.D.

Acknowledgement is made to the donors of the Petroleum Research Fund, administered by the American Chemical Society, for partial support of this research under PRF Grant Number 2744B. The authors wish to acknowledge the assistance of their students: G. Swanson, H. Prieto and G. Smith.

Appendix

In order to formulate an expression for the work of forming the depression, the process is visualized as the process of increasing the capillary velocity from zero to the velocity, $u_c(r)$, necessary to give the final depression, $h(r)$. There corresponds a steady-state velocity $u(r, h_1)$ for each intermediate indention depth h_1, which allows the work expression to be formulated as

$$w_1 = K \int_0^R \int_0^h \rho_g u^2(r, h_1)\, 2\pi r\, dh_1\, dr. \tag{15}$$

Experimental determination of the functional dependence of $u(r, h_1)$ indicates that it is separable, i.e.

$$u(r, h_1) = u_c(r) f(h_1). \tag{16}$$

Using the indention data to make plots of $f(h_1)$ versus h_1/h for various r between 0 and R_c, it was found that $f(h_1)$ for all r and all surface tensions used could be expressed by

$$f^2(h_1) = 2(h_1/h) - (h_1/h)^2. \tag{17}$$

Using equations (16) and (17) to carry out the inner integration in (15), and equating the result to (1*a*) gives, after rearrangement, an expression for the evaluation of $\bar{h}$ (laminar flow – parabolic capillary profile)

$$\bar{h} = \frac{4}{R_c^6} \int_0^{R_c} h(R_c^2 - r^2)^2 r\, dr. \tag{18}$$

REFERENCES

BANKS, R. B. & CHANDRASEKHARA, D. V. 1962 Experimental investigation of the penetration of a high-velocity gas jet through a liquid surface. *J. Fluid Mech.* **15**, 13.

COLLINS, R. D. & LUBANSKA, H. 1954 The depression of liquid surfaces by gas jets. *Br. J. Appl. Phys.* **5**, 22.

GIBSON, A. H. 1934 *Hydraulics and Its Application.* London: Constable.

MATHIEU, F. 1960 Contribution a l'étude de l'action d'un jet gazeux sur la surface libre d'un liquide. *Rev. Universelle des Mines*, **16**, 7, 309.

MATHIEU, F. 1962 Nouvelles recherches sur l'action d'un jet gazeux sur la surface libre d'un liquide au repos. *Rev. Universelle des Mines*, **18**, 7, 482.

PFUND, A. H. & GREENFIELD, E. W. 1936 Surface tension measurements of viscous liquids. *Ind. Engng. Chem.* **8**, 1, 81.

TURKDOGAN, E. T. 1966 Fluid dynamics of gas jets impinging on surface of liquids. *Chem. Engng. Sci.* **21**, 12, 1133.